ISMRM 19th Annual Meeting (Montreal, May 2011) – Abstract
Graeme M. Bydder, MB, ChB ~ University of California San Diego
Nouvelle Techniques in Current Clinical Use
Tuesday – 10 May 2011 (13:30)

"Clinical Imaging of Short T2/T2* Tissues"

Graeme M Bydder, Department of Radiology, University of California San Diego, 200

West Arbor Drive, San Diego, CA 92103-8226 USA

Phone: 619-471-0506

Fax: 619-471-0503

Email: gbydder@ucsd.edu

SUMMARY

There are now a variety of new techniques available to detect signal from tissues with short or ultrashort T2s and T2*s. There are also many methods of developing image contrast between tissues in the short or ultrashort T2 or T2* range which can provide visualization of anatomy and pathology which has not previously been seen. Particular methods have been developed to target susceptibility effects and provide accurate quantitation by compensating for anatomic distortion produced by these effects. Specific methods have been developed to image the effects of magnetic iron oxide particles with positive contrast. It is also possible to correct for loss of signal and image distortion near to metal due to gross susceptibility effects. These methods are likely to increase the range of applications of MR imaging.

KEYWORDS: Short T2 Tissue Components, Susceptibility, Ultrashort Echo Time

FINANCIAL DISCLOSURE/ACKNOWLEDGEMENTS:

The author has received grant support from General Electric Healthcare.

1 INTRODUCTION

During the first year of clinical MR imaging only steady state free precession, T1-weighted and proton density-weighted clinical images were available [1-3]. Heavily T2-weighted spin echo (SE) sequences arrived suddenly in early 1982 and transformed the practice of MR [4-6]. Images obtained with these sequences detected intermediate or long T2 relaxation components in tissue. Even with the subsequent development of new classes of sequences such as fast SE, clinical diffusion weighted imaging and fluid attenuated inversion recovery, detection of signal from intermediate and long T2 relaxation components remains the dominant form of MR imaging for diagnosis of parenchymal disease in the brain and much of the rest of the body.

However even when clinical MR imaging began very short mean T2 relaxation components were recognized in cortical bone by Smith et al [7] and Edelstein et al [8]. This tissue showed no MR signal. The lack of signal was useful in providing a low signal background against which abnormalities in cortical bone with mean T2s sufficiently long to result in detectable signal could be recognized, but the absence of signal from normal cortical bone meant that there was no possibility of measuring normal values of mobile proton density (ρ_m), T1, or T2. Nor was it possible to study normal perfusion, and there was no opportunity for active contrast manipulation, little or no distinction between adjacent short T2 tissues, and no means of visualizing normal contrast enhancement. As a result study of cortical bone and other MR "invisible" short mean T2 tissues such as tendons, ligaments and menisci has been far more limited than that of tissues and organs such as brain, liver and muscle where tissue mean T2s are longer and MR signal from them can be readily detected with conventional clinical sequences. However even these longer mean T2 tissues contain significant proportions (e.g., 5-30%) of

"invisible" or undetectable short T2 relaxation components when they are imaged with conventional approaches.

To image short or ultrashort mean T2 tissues which produce no detectable signal with conventional sequences indirect methods have been used in which signal is obtained from surrounding or associated longer T2 tissues. When the low or zero signal tissue is surrounded by longer T2 tissue, signal from the latter tissue can be used to define the boundaries of the zero signal tissue. It is also possible to characterize some short T2 tissues by observing the impact their difference in susceptibility from that of a surrounding longer T2 tissue has on the signal obtained from the longer T2 tissue. For example some features of trabecular bone can be inferred by the effect this tissue has on the MR signal of adjacent red or yellow bone marrow [9]. A third indirect method of imaging short T2 components is possible when short and long T2 relaxation components are associated, and undergo magnetization exchange. The effect of saturation of the invisible short T2 components on this exchange can be observed on the signal from the detectable longer T2 components [10] and so inferences can be made about the short mean T2 tissue and/or the exchange between the shorter and longer T2 tissue components.

An alternative to using conventional sequences to study short T2 tissues in these indirect ways is to employ methods which directly detect signal from them. These usually involve the use of short or ultrashort echo time (UTE) sequences so that their MR signals can be detected before they have decay to zero. There are now a variety of sequences of this type available in the clinical domain.

While T2 is a property of tissue which reflects dipolar and other nuclear (and electronic) interactions, frequently the effects seen with MR imaging are described more accurately by the observed T2, or T2*. This includes effects such as intravoxel dephasing due to Bo field inhomogeneity, tissue susceptibility differences, and chemical shift. Tissue susceptibility effects reflect the fact that solid tissues such as bone are generally more diamagnetic than soft tissues and that some tissues and fluids may be paramagnetic. The effects of some of these differences can be partly or almost wholly reversed by the use of spin echo (SE) sequences.

In some situations T2* effects may dominate and it is useful to recognize several different approaches to imaging of short T2/T2* components of tissue, fluid and materials.

(i) The first approach essentially sees the problem as one of imaging short or ultrashort T2 components and the basic approach has been to use short or ultrashort TEs to acquire and encode MR signals before they decay to a low level. This may be appropriate in situations where they are only minor tissue susceptibility effects present.

(ii) The second is magnetization transfer (MT) in which typically shorter T2 components are partially or completely saturated and the effect of this on longer (detectable) T2 components is observed. With short T2 tissues, and short and ultrashort TE data collections the definition of shorter and longer T2 components may change. Also off resonance MT pulses may directly saturate short T2 components of interest.

(iii) The third is susceptibility weighted imaging (SWI), where magnitude and/or phase data are used to recognize loss or change of signal from tissue due to susceptibility

effects. It can be direct and/or indirect (where tissue T2s* become too short to detect) and is qualitative. Quantitative Susceptibility Imaging or Susceptibility Mapping recognizes the fact that susceptibility differences effect slice selection and frequency encoding of MR signals and endeavours to correct for this, and to calculate values of T2* which accurately reflect both T2 and susceptibility effects.

(iv) Positive Contrast and White Marker Imaging. These techniques address the specific problem of imaging the effects of magnetic iron oxide particles (MIOPs) which shorten T2 and produce local disturbances of the magnetic field. The aim is to detect the presence of particles with positive signal, and at least in part address the problem of field distortion and so achieve credible recognition and quantification of the concentration of MIOPs.

(v) The fifth group of techniques is targeted at imaging in the presence of metal. Metals may have very large susceptibility differences from tissues and can produce very large susceptibility effects with loss of signal due to T2* shortening and gross image distortion. The primary objective in this situation is to deal with the image distortion and restore image integrity to a sufficient degree to make the images clinically useful.

There is overlap between these approaches, and they may be combined. In some situations it may be appropriate to ignore the effects of susceptibility differences in producing image distortion and regard the problem as one of detecting short T2 signals whereas in other situations image distortion due to susceptibility is the primary problem that needs to be addressed. Over the last year there has been considerable interest in these approaches and there are now solutions or partial solutions available to problems that have appeared intractable for many years.

2 TISSUE, FLUID AND MATERIAL PROPERTIES

The tissues of the human body can be divided into those that are "visible" in the sense that they provide detectable signal with clinical MR systems and those that are "invisible" because their mean T2s or T2*s are too short to provide a detectable signal. All tissues have multicomponent T2s. This means that they contain a mixture of short and long T2 components. The invisible tissues have a majority of short T2 components and a minority of long T2 components. The latter components typically do not provide enough signal to be detectable in relation to image noise levels. The "invisible" tissues of the body such as brain, liver and muscle have a majority of long T2 components which produce signal with conventional techniques. They also have a minority of short T2 components which do not contribute significantly to the detectable signal.

There is no agreement as to what constitutes a short TE and what is an ultrashort TE, and there is argument about how TE should be measured for tissues with short T2s (11-13), but for simplicity, a short TE is taken to be less than 10 ms and an ultrashort one to be less than 1 ms. It is also possible to define short T2/T2* as less than 10 ms and ultrashort as less that 1 ms. This reflects the fact that with older systems and SE sequences tissues with T2 or T2* less than 10 ms produced little or no signal and were "invisible". With more recent systems and gradient echo sequences the cut off is closer to 1 ms.

Within the invisible group of tissues (mean T2 < 10ms) it is possible to differentiate a first group including tendons, ligaments, and menisci with short mean T2s of about 1-10 ms, a second group including cortical bone and dentine with ultrashort mean T2s of 0.1-1 ms. There is also a third

group including dental enamel, protons in membranes, and molecules as well as crystalline bone with super short mean T2s of less than 0.1 ms. Materials can also be classified in a similar way.

An important factor in this context is the magic angle effect [14,15] since it can greatly increase the T2 of short T2 tissues such as tendons, ligaments and meniscii. When the orientation of tissues which contain highly ordered collagen is changed their T2 varies from a minimum at $\theta = 0°$ where dipolar interactions are greatest, to a maximum where $3\cos^2\theta - 1 \approx 0$ and $\theta = 55°$. θ is the orientation of the fibers to Bo. The increase can be large, for example from 0.6 ms to 21 ms [14] or from 7 to 23 ms [15] in the Achilles tendon.

A recently described phenomenon is directional susceptibility in tendons whereby their bulk magnetic susceptibility varies with orientation to Bo with signals at the water end of the proton spectrum when fibers are parallel to Bo and at the fat end of the spectrum (lower frequency) when fibers are perpendicular to Bo [16]. The difference is relatively large (of the order of three parts per million).

The ρ_m of tissues also varies markedly with bone having a ρ_m of 15-20% and semi-solid tissues such as tendons and ligaments values of 60-70%. ρ_m is generally a more important factor in generating contrast with short T2 tissues than it is with longer T2 tissues. The low ρ_m for bone places a limit on the maximum signal than can be obtained from it.

The mean T1s of some tissues with a majority of short T2 components are short with cortical bone having a particularly short T1, in fact less than that of fat [17]. The relative differences in

mean T2 or T2* between normal and abnormal tissue are generally much greater than those in mean T1.

Relative to air, soft tissues generally show a susceptibility difference of about -9 ppm (parts per million), and bone and calcified tissue about -11 ppm. By comparison the principal peak of fat resonates at about -12 ppm. Paramagnetic materials show small positive frequency shifts and superparamagnetic materials greater positive shifts. Metals including, for example, titanium, metal alloys and some types of stainless steel may show very large positive shifts of 10s to 1000s of ppm. These changes in field may be considerably greater than those of machine gradient fields used to encode MR signals and may therefore cause image distortion.

In disease increases in T2 are frequently seen but decreases in T2 may be seen with increased iron content and in other disease processes. Loss of magic angle effect may be seen in degeneration and fibrosis.

3 ACQUISITION METHODS FOR SHORT T2/T2* COMPONENTS

Some of the techniques now being used to directly detect signal from tissues on clinical systems have been used in materials science and tissue studies using small bore high field spectrometers for many years. Methods now in use on lower performance clinical systems are summarized in Table 1. The prototype sequence for imaging short T2 tissues is Single Point Imaging (SPI) where a single point in k-space is acquired with an ultrashort TE. This is typically used with 3D phase encoding which unfortunately makes the technique time consuming even with optimized k space sampling [18].

It is possible to acquire several points at a time which makes the sequences more time efficient but results in longer TEs for the additional points [19]. There are also Free Induction Decay (FID) based techniques where a radial line of k-space is acquired from the centre out [20]. This can be coupled with long T2 water and fat suppression to selectively image short T2 components [21]. Other trajectories in k-space are possible including a Stack of Spirals [22].

A particularly innovative method of imaging short T2 components is to divide the excitation pulse into subpulses and acquire data after each of these pulses. This is known as Swift Imaging with Fourier Transformation (SWIFT) or Simultaneous Excitation and Acquisition (SEA). The acquired data needs to be deconvolved with the excitation pulse, but the end result is a much more time efficient acquisition than with typical 3D acquisitions [23-26]. Other techniques which have only been used in the pre-clinical phase include methods in which radiofrequency (rf) absorption is assessed rather than signal detection [27]. The methods borrow from continuous wave spectroscopy and electron spin resonance where electronic T2s are extremely short and may be of the order of a microsecond.

4 MAGNETIZATION PREPARATION AND PULSE SEQUENCES SIGNAL SUPPRESSION TECHNIQUES

Traditional contrast mechanisms exploiting differences in $\rho_{m,}$ chemical shift and other tissue properties can be used in ways that are well known from conventional imaging.

There are also numerous old contrast mechanisms operating in new ways as well as new contrast mechanisms that are of interest in imaging short/ultrashort T2/T2* components in tissue. Some of these are listed in Table 2. They are typically used in conjunction with the acquisition

techniques mentioned in the previous section. These provide a wide range of possible ways of effecting magnetization. For example, 90°, 180°, fat saturation and magnetization transfer pulses can all be used to suppress unwanted long T2 signals and to produce T2 contrast in the short T2 range. There are also quite new potential mechanisms (as far as clinical imaging is concerned) involving reductions in dipolar coupling [28, 29] and double quantum filters [30]. These techniques are usually used in conjunction with one of the acquisition methods described in the previous section.

5 MAGNETIZATION TRANSFER (MT)

This differs for clinical approaches in that use of short TE acquisitions makes it possible to study MT in tendons, ligaments, menisci and cortical bone [31]. The definition of the bound (short T2) and free (long T2) pools may change because previously undetected signals are included in the free (detectable) pool. Direct saturation is a greater problem. There may also be a greater degree of magnetization exchange present in short mean T2 tissues. The technique provides indirect access to ultrashort and even supershort T2 relaxation components in tissues with super short T2s of about 5-15 μs which are not directly accessible with most UTE techniques.

6 SUSCEPTIBILITY WEIGHTED IMAGING

Susceptibility weighted imaging has been in use for a considerable time. It usually exploits reductions in T2* to develop contrast and imaging may utilize both magnitude and phase data [32, 33]. The T2* may be so short that this becomes in effect an indirect form of imaging utilizing the reduction in signal of adjacent longer T2 components. The applicability of the technique and related methods can be expanded by utilizing forms of data collection with short

or ultrashort TEs that can detect signal from very short T2* components [34,35]. Quantitative methods of imaging susceptibility changes need to account for errors in spatial encoding which may require solutions to a complex inverse problem [36, 37]. To date it has mainly been applied to brain imaging. Phase and frequency changes can be detected in fibrous structures even with UTE sequences [35].

7 POSITIVE CONTRAST AND WHITE MARKER IMAGING

These forms of imaging have been used to describe the particular situation with MIOPs which may not only reduce T2 and T2* but produce local field distortions. A variety of different methods are available. It is possible to selectively excite only off resonance spins. It is also possible to apply an additional gradient so that only the magnetization of spins in regions affected by MIOPs is refocused. The inhomogeneities from the particles induce echo shifts and these can be used to calculate and correct for the field distortion. The images reflect both tissue MIOP concentration and deviations of the local magnetic field produced by the particles [38-42]. Techniques using SWIFT [43] and UTE [44, 45] have also been successful for imaging MIOPs.

8 IMAGING IN THE PRESENCE OF METAL

When forms of metal are implanted in the body an extreme situation may arise in which there is very marked T2* shortening but the image distortion is so great that images of regions adjacent to the metal are uninterpretable. This has been a longstanding problem. A variety of solutions have been proposed in the past, but these have had relatively little clinical impact. The recent development of Multi-Acquisition Variable-Resonance Image Combination (MAVRIC) [46], and Slice Encoding for Metal Artefact Correction (SEMAC) [47] has resulted in a remarkable

degree of restoration of images which are grossly degraded by metallic artefact when imaged using conventional approaches. With MAVRIC irradiation at a range of different off resonance frequencies is used to detect signals whose resonant frequency has been shifted by metal, and these are then combined. With SEMAC, phase encoding is used during slice selection to reallocate signals that are improperly located by the slice selection process. View angle tilting (VAT) [48] is also used with this technique to correct for errors with in plane spatial encoding. Faster versions [49] and a MAVRIC -SEMAC hybrid [50] have also been implemented. UTE alone shows some improvement over conventional techniques but this may be less than that available with [51] SEMAC and/or MAVRIC.

9 IMAGING OF BOUNDARIES INVOLVING SHORT T2/T2* TISSUES

Structures of interest in the short T2 range include thin layers such as those in entheses, periosteum and the deep layers of articular cartilage where there are short T2 tissues, susceptibility effects between the soft (or semi-solid) tissues and bone, as well as partial volume effects between these tissues which are present over curved surfaces. In this situation high resolution 3D isotropic UTE imaging often has a distinct advantage since it can detect short T2/T2* signals as well as reduce the impact of susceptibility differences and partial volume effects. Imaging of ordered fibrous structures such as tendons and ligaments include some of the above issues, but in addition loss of contrast of the fiber structure or "blurred" appearance may arise from obliquity of the fibers relative to the imaging slice. This effect may simulate changes due to disease. There are also distinctive artefacts at boundaries from chemical shift effects including those associated with radial acquisitions.

10 CLINICAL PROTON APPLICATIONS

There are now 2D and 3D UTE sequences available with imaging times of 5-6 minutes and clinically acceptable spatial resolution [e.g., 22, 52]. In general the difficulty of acquiring short/ultrashort T2/T2* signals means that invisible tissues are imaged at lower spatial resolution, but with signal levels and contrast that are not attainable with conventional techniques. There is a balance necessary to obtain qualitative and/or quantitative information which is novel at spatial resolutions that are sufficient to show anatomic features with acceptable clarity.

Cortical Bone

Cortical bone can be demonstrated with high signal [17]. Its T2 is about 0.4 ms and T1 250-350 ms at 1.5T which is shorter than typical values for fat. Its mobile proton density is about 15-20%. Detectable signal can be used both for quantitative and qualitative studies [53-55] [see Fig 1] as well as comparison with spectroscopic studies [56]. UTE measurements of bone may be of value for attenuation corrections in PET/MRI [57, 58].

Tendons, Ligaments, and Entheses

With conventional sequences the signal from tendons, ligaments and entheses is very low or zero. Entheses are the attachment sites of tendons, ligaments and capsules to bone. They typically contain calcified and uncalcified fibrocartilage (which both have short T2s). These tissues have a major role in dispersing mechanical stress at the junction between flexible tendons or ligaments and rigid bone.

Tendons and ligaments contain endotenon and endoligament which have longer T2s than the fibrous components (although they are still in the short T2 range) and less magic angle effect. Uncalcified fibrocartilage has a longer T2 than the tensile components of tendons as well as an increase in T2 due to the magic angle effect although this may be present over a wider range of angles reflecting the more dispersed arrangement of the fibers within it. Magic angle effects may result in a pronounced longer T2 line adjacent to bone from fibers which change in direction from parallel to the bone surface to perpendicular to it as they insert into bone.

Tendons and ligaments can readily be seen with UTE sequences and entheses have been studied in detail [59, 60]. Off resonance fat suppression pulses reduce the signal from short T2 fibers (which have a broad line width) more than endotenon, or enthesis fibrocartilage (which have longer T2s and narrower linewidths) and this can be an effective contrast mechanism. Inversion pulses may be used to selectively invert and null enthesis fibrocartilage (exploiting its longer T2) and so visualize this tissue with high contrast. It is also possible to visualize oblique and transverse fibers in tendons using a combination of fat suppressed UTE sequences to reduce short T2 tissue water components and magic angle imaging to lengthen the T2 of the fibers at particular angles to B_0 (Fig 2).

Entheses are selectively involved in the seronegative spondyloarthropathies such as ankylosing spondylitis and psoriatic arthropathy. The differential diagnosis is of a loss or reduction in fascicular pattern and includes normal sesamoid fibrocartilage, partial volume effects with a loss of fascicular pattern due to partial volume effects, magic angle effects and disease.

The menisci of the knee

The central region of the adult meniscus has no blood supply (the white zone) while the more peripheral region (the red zone) has a blood supply. Healing of tears in the white zone is generally unsatisfactory and the preferred surgical strategy is usually resection of the torn tissue. Suture and repair is more successful in the red zone. Distinction between the two zones has not previously been possible with MR imaging using conventional sequences in spite of repeated attempts [61]. Using UTE sequence and gadolinium based contrast enhancement the two zones can be distinguished [62] and provide a basis for surgical planning.

Anatomic descriptions of the meniscus include circumferential, radial, lamella, vertical and meshwork fiber groups. With conventional imaging some radial fibers may be distinguishable from the majority of circumferential fibers [61] but with UTE and magic angle imaging each of these fiber groups can be identified (e.g., Fig 3) [63-66]. It is also possible to distinguish the internal structure of the meniscus from that of the root ligaments, and the more central cartilaginous region from the peripheral more fibrous region of the meniscus.

The fiber structure provides a basis for understanding the biomechanics of the knee and the various patterns of tear in the meniscus. It also helps in distinguishing magic angle effects within fiber groups from degenerative changes. Quantitative studies of $T_1\rho$ and T2 may be informative [67, 68].

The temporomandibular joint disc shows some of the characteristics of the meniscus of the knee. Fiber structure can be seen. Lamella, circumferential antero-posterior and superior-inferior fibers are identifiable.

Articular cartilage

Articular cartilage has a range of T2s from about 1 to 30-40 ms from deep to superficial. With conventional imaging the deep radial and calcified layers as well as the adjacent subchondral bone are invisible. With UTE imaging signal is detectable from the deeper layers of cartilage allowing more superficial cartilage and subchondral bone to be distinguished [69-71]. This provides a basis for study of the junction between cartilage and bone which may be of importance in the pathogenesis of osteoarthritis. Complex magic angle effects are seen because of the fibrous architecture of articular cartilage.

In disease there may be both loss of signal from the deep layer and increased extent of the short T2 associated with deep layers. There is electron microscope evidence of thinning of the deep layers in osteoarthritis but preservation in osteomalacia.

The spine

Imaging of the spine includes many visible tissues so that attention to date has focused on invisible structures such as (i) entheses (ii) the end plate of the disc, and (iii) short T2 components in the intervertebral discs and red bone marrow. Fibrocartilage has also been demonstrated in the functional entheses of the transverse ligament of the Atlas and the alar ligament. The dorsal capsule of the facet joints of the lumbar spine are also subject to cartilagenous metaplasia. Evidence of iron deposition can be seen in intervertebral discs in

thalassemia [72]. Sclerotic metastases have been identified [73] as well as cement after vertebroplasty [74].

Central Nervous System

There are significant short T2 components in many tissues of the body with longer mean T2s including brain, spinal cord and peripheral nerve. These components can be specifically detected using UTE and other acquisition methods coupled with techniques which suppress long T2 signals [75-77]. It is possible to specifically image short T2 components in myelin and use these to map white matter and identify disease [78-81].

Lung

Imaging of the lung was the first application of UTE imaging [20]. More recent studies have identified emphysema, cystic fibrosis and other conditions [82-85].

Liver

The liver contains a relatively high proportion of short T2 components. The T2*s of these may be prolonged in fibrosis [86]. Fibrosis in this situation is often of a relatively open structure and includes free water.

Pelvis

UTE sequences have found application in studying the effects of cryosurgery in carcinoma of the prostate [87]. Freezing of tissues results in a substantial reduction in T2* [88].

Atherosclerotic Plaque

Short T2 components and calcification have been identified and characterized in atherosclerotic plaque [89-91].

11 OTHER PROTON APPLICATIONS

Contrast enhancement with Gadolinium chelates may be seen within previously invisible tissues using UTE sequences [92] as well as with MIOPs [38-45]. Dental imaging has successfully identified caries [93, 94]. Mummified tissue has also been studied [95].

12 OTHER NUCLEI

Sodium imaging has a long history with the principal applications in the brain [96-100], heart [100] and musculoskeletal system [102-104]. Phosphorus imaging has also been performed with UTE sequences [105]. Oxygen-17 studies have been performed in the brain [99, 100].

13 QUANTITATIVE APPROACHES

Quantitation may include specific MR properties including in particular T2 and T2* [e.g., 106-108], the properties of the remaining signal after long T2 components are suppressed, and the ratio of short T2 to long T2 components. There are also other features such as the magic angle effect and dipolar contrast that can be characterized [109-111].

There are issues about measuring T2 and T2* in the correct range, characterizing different T2 components (e.g., long and short) including their relative proportions and dealing with artefacts from various sources. However quantitation may be confounded by slice selection and eddy

current problems and by contamination of short T2 components with long T2 components which are present in higher concentration.

14 ARTEFACTS

Short time constant eddy currents and gradient timing errors may result in artefacts and errors in measurement which can be corrected [112-115].

15 CONCLUSION

Imaging of short T2 and T2* components is a rapidly expanding area which has seen a convergence of imaging methods targeted at tissues with short T2 components, susceptibility weighted imaging, MIOP imaging and metal artefact control. The methods have borrowed from solid state imaging, spectroscopy including continuous wave methods, electron spin resonance and MR microscopy. The much lower technical performance of clinical systems compared with small bore spectrometers is a major limitation, but innovative methods for overcoming this problem are now being developed.

The tissues of interest have mainly been in the musculoskeletal system but all tissues of the body have some short T2 components and study of these may prove to be of diagnostic importance. Some techniques such as imaging in the presence of metal are likely to be immediately useful in the clinical domain while others may require validation and comparative assessment to establish their role. Quantitative approaches may be useful given the large fractional changes in short T2 and T2* components that may be seen in disease. The techniques used for imaging often require high gradient performance with control of short term eddy currents to a level not previously

necessary in clinical MR systems. In spite of these and other technical difficulties, application to the study of short T2 and T2* tissues appears likely to be an area of MR imaging of considerable importance in the near future.

Table 1 - Short and Ultrashort TE Imaging Techniques		
Technique	Radiofrequency pulses and gradient	k-space trajectory
Single point (18)	Non selective hard pulse with gradient applied	3D point by point
Multipoint (19)	Hard pulse with gradient applied	3D partial lines Several points
UTE (20, 116)	2D two half pulses 3D hard pulse No gradient applied during rf	Radial from center out FID acquisition
WASPI (21)	3D hard pulse with gradient on. Preparation pulses with water and fat signal suppression	Radial from center out, FID acquisition
Gradient echo	2D, 3D	Radial rephasing gradients
Cones (117) Spiral (118) Stack of spirals (22) Echo Planar Imaging (119) bSSFP (84)	3D	Spiral, from center out, FID data collection
SWIFT, SEA (23-26)	3D rf sub-pulses	Radial, center out

Table 2 – Magnetization Preparation, Pulse Signal Suppression Techniques and Pulse Sequences	
Mechanism	Effect
90° pulse	Selective excitation of short T2/T2* components with or without subsequent long T2 signal suppression
180° pulse [120-124]	Selective excitation of short T2/T2 components and inversion of long T2 components
180° pulse and nulling [124]	Selective inversion of long T2/T2* components with nulling
Off resonance saturation [125]	Selective reduction of short T2 components
Magnetization transfer (MT) [30]	Selective reduction of short T2 components with MT to detectable T2 components
Fat saturation	Selective reduction of fat and short T2/T2* water signals
Later image subtraction from first image [126]	Selective reduction of long T2/T2* components
Susceptibility and spectral mapping UTESI [34, 35]	Direct mapping of field and frequency change as well as susceptibility differences
R* – IDEAL – UTE [52]	Combination of fat suppression and R2* measurement of short T2/T2 components
Double quantum filter [30]	Comparison of spin echo and magic sandwich echo imaging
Dipolar imaging [28, 29]	Selective imaging of protons with strong unaveraged dipolar coupling
Dipolar Anisotropy Fiber Imaging [111]	Systematic exploration of signal at different orientations of fibers to B_0 application in short T2 tissues
$T_1\rho$ imaging [67]	Applicable to short T2 tissues
$T_2\rho$ imaging [127]	T2 in the rotating frame
Phase shift due to flow can be specifically targeted [128]	Detection and measurement of high velocity flow

REFERENCES

1 – Hawkes RC, Holland GN, Moore WS, Worthington BS. Nuclear magnetic resonance (NMR) tomography of the brain: a preliminary clinical assessment with demonstration of pathology. J Comput Assist Tomogr 1980; 4:577-86.

2 – Smith FW, Mallard JR, Hutchison JM, Reid A, Johnson G, Redpath TW, Selbie RD. Clinical application of nuclear magnetic resonance. Lancet 1981; 1(8211) 78-9.

3 – Young IR, Hall AS, Pallis CA, Legg NJ, Bydder GM, Steiner RE. Nuclear magnetic resonance imaging of the brain in multiple sclerosis. Lancet 1981; 2(8255) 1063-6.

4 – Bailes DR, Young IR, Thomas DJ, Straughan K, Bydder GM, Steiner RE. NMR imaging of the brain using spin-echo sequences. Clin Radiol 1982; 33:395-414.

5 – Bydder GM, Steiner RE, Young IR *et al*. Clinical NMR imaging of the brain: 140 cases. AJR Am J Roentgenol 1982; 139:215-236.

6 – Crooks LE, Mills CM, Davis PL *et al.* Visualization of cerebral and vascular abnormalities by NMR imaging. The effects of imaging parameters on contrast. Radiology 1982; 144:843-852.

7 – Smith FW. Clinical application of NMR tomographic imaging. In: *NMR Imaging*. Witcofski RL, Karstaedt N, Partain CL, (Eds), Bowman Gray School of Medicine, Winston Salem, NC, 1982; 125-132.

8 – Edelstein WA, Bottomley PA, Hart HR, et al. NMR imaging at 5.1 MHz: work in progress. In: *NMR Imaging*. Witcofski RL, Karstaedt N, Partian CL (Eds), Bowman Gray School of Medicine, Winston Salem, NC, 1982; 139-145.

9 – Wehrli FW, Song HK, Saha PK, Wright AC. Quantitative MRI for the assessment of bone structure and function. NMR in Biomed 2006; 19:731-64.

10 – Henkelman RM, Stanisz GJ, Graham SJ. Magnetization transfer in MRI: a review. NMR in Biomed 2001; 14:57-64.

11 – Robson MD, Gatehouse PD, Young IR, Bydder GM. Ultrashort TE (UTE) imaging of short T2 relaxation components: how should the T2 weighting be described? Proc Intl Soc Mag Reson Med 11 2004; p636.

12 – Robson MD, Gatehouse PD. Consequences of T2 relaxation during half-pulse slice selection for ultrashort TE imaging. Magn Reson Med 2010; 64:610-5.

13 – Springer F, Steidle G, Martirosian P, Claussen CD, Schick F. Effects of in-pulse transverse relaxation in 3D ultrashort echo time sequences: analytical derivation, comparison to numerical simulation and experimental application at 3T. J Magn Reson 2010; 206:88-96.

14 – Fullerton GD, Cameron IL, Ord VA. Orientation of tendons in the magnetic field and its effect on T2 relaxation times. Radiology 1985; 155:433-35.

15 – Henkelman RM, Stanisz GJ, Kim JK *et al*. Anisotropy of NMR properties of tissue. Magn Reson Med 1994; 32:592-602.

16 – Krasnosselskaia LV, Fullerton GD, Dodd SJ, Cameron IL. Water in tendon: orientational analysis of the free induction decay. Magn Reson Med 2005; 54:280-288.

17 – Reichert ILH, Robson MD, Gatehouse PD *et al.* Magnetic resonance imaging of cortical bone with ultrashort TE pulse sequences. Magn Reson Imaging 2005; 23:611-618.

18 – Chen Q, Halse M, Balcom BJ. Centric scan SPRITE for spin density imaging of short relaxation time porous materials. Magn Reson Imaging 2005; 23:263-6.

19 – Fernandez-Seara MA, Wehrli SL, Wehrli FW. Multipoint mapping for imaging of semi-solid materials. J Magn Reson 2003; 160:144-150.

20 – Bergin CJ, Pauly JM, Macovski A. Lung parenchyma: projection reconstruction MR imaging. Radiology 1991; 179:771-781.

21 – Wu Y, Ackerman JL, Chesler DA, Graham L, Wang Y, Glimcher MJ. Density of organic matrix of native mineralized bone measured by water-and-fat suppressed proton projection MRI. Magn Reson Med 2003; 50:59-68.

22 – Qian Y, Boada FE. Acquisition-weighted stack of spirals for fast high-resolution three-dimensional ultra-short echo time MR imaging. Magn Reson Med 2008; 60:135-45.

23 – Idiyatullin D, Corum C, Park JY, Garwood M. Fast and quiet MRI using a swept radiofrequency. J Magn Reson 2006; 181:342-349. Epub 2006 Jun 19.

24 – Idiyatullin D, Corum C, Moeller S, Garwood M. Gapped pulses for frequency-swept MRI. J Magn Reson 2008; 193:267-73. Epub 2008 May 20.

25 – Blümlich B, Gong Q, Byrne E, Greferath M. NMR with excitation modulated by Frank sequences. J Magn Reson 2009; 199:18-24. Epub 2009 Mar 28.

26 – Weiger M, Hennel F, Pruessmann KP. Sweep MRI with algebraic reconstruction. Magn Reson Med 2010; 64:1685-95.

27 – Fagan AJ, Davies GR, Hutchison JM, Glasser FP, Lurie DJ. Development of a 3-D multi-nuclear continuous wave NMR imaging system. J Magn Reson 2005; 176:140-150.

28 – Grenier D, Pascui O, Briguet A. Dipolar contrast for dense tissues imaging. J Magn Reson 2000; 147:353-6.

29 – Regatte RR, Schweitzer ME, Jerschow A, Reddy R. Magic sandwich echo relaxation mapping of anisotropic systems. Magn Reson Imaging 2007; 25:433-8. Epub 2006 Nov 20.

30 – Navon G, Eliav U, Demco DE, Blümich B. Study of order and dynamic processes in tendon by NMR and MRI. J Magn Reson Imaging 2007; 25:362-80.

31 – Springer F, Martirosian P, Machann J, Schwenzeer NF, Claussen CD, Schick F. Magnetization transfer contrast imaging in bovine and human cortical bone applying an ultrashort echo time sequence at 3 Tesla. Magn Reson Med 2009; 61:1040-1048.

32 – Haacke EM, Mittal S, Wu Z, Neelavalli J, Cheng YC-N. Susceptibility-weighted imaging: technical aspects and clinical applications, part 1. AJNR Am J Neuroradiol 2009; 30:19-30.

33 – Mittal S, Wu Z, Neelavalli J, Haacke EM. Susceptibility-weighted imaging: technical aspects and clinical applications, part 2. AJNR Am J Neuroradiol 2009; 30:232-52.

34 – Du J, Chiang AJ, Chung CB, Statum S, Znamirowski R, Takahashi A, Bydder GM. Orientational analysis of the Achilles tendon and enthesis using an ultrashort echo time spectroscopic imaging sequence. Magn Reson Imaging 2009.

35 – Du J, Carl M, Bydder GM. "Ultrashort TE Imaging: Phase and Frequency Mapping of Susceptibility Effects in Short T2 Tissues of the Musculoskeletal System" Ed by E.M. Haacke, J.R. Reichenbach in *Susceptibility Weighted Imaging: Basic Concepts and Clinical Applications* 2011 by Wiley-Blackwell (in press).

36 – Schäfer A, Wharton S, Gowland P, Bowtell R. Using magnetic field simulation to study susceptibility-related phase contrast in gradient echo MRI. Neuroimage 2009; 48:126-37.

37 – de Rochefort L, Liu T, Kressler B, Liu J, Spincemaille P, Lebon V, Wu J, Wang Y. Quantitative susceptibility map reconstruction from MR phase data using bayesian regularization: validation and application to brain imaging. Magn Reson Med 2010; 63:194-206.

38 – Cunningham CH, Arai T, Yang PC, McConnell MV, Pauly JM, Conolly SM. Positive contrast magnetic resonance imaging of cells labeled with magnetic nanoparticles. Magn Reson Med 2005; 53:999-1005.

39 – Suzuki Y, Cunningham CH, Noguchi K *et al.* In vivo serial evaluation of superparamagnetic iron-oxide labeled stem cells by off-resonance positive contrast. Mag Reson Med 2008; 60:1269-1275.

40 – Liu W, Frank JA. Detection and quantification of magnetically labeled cells by cellular MRI. Eur J Radiol 2009; 70:258-264.

41 – Dahnke H, Liu W, Herzka D, Frank JA, Schaeffter T. Susceptibility gradient mapping (SGM): A new postprocessing method for positive contrast generation applied to superparamagnetic iron oxide particle (SPIO)-labeled cells. Magn Reson Med 2008; 60:595-603.

42 – Liu W, Dahnke H, Rahmer J, Jordan EK, Frank JA. Ultrashort T2* relaxometry for quantitation of highly concentrated superparamagnetic iron oxide (SPIO) nanoparticle labeled cells. Magn Reson Med 2009; 61:761-766.

43 – Zhou R, Idiyatullin D, Moeller S et al. SWIFT detection of SPIO-labeled stem cells grafted in the myocardium. Magn Reson Med 2010; 63:1154.61.

44 – Crowe LA, Wang Y-X, Gatehouse P, Tessier J, Waterton J. Robert P, Bydder G, Firmin DN. Ex vivo MR imaging of atherosclerotic rabbit aorta labeled with USPIO – Enhancement of iron loaded regions in UTE imaging. Proc Intl Soc Mag Reson Med 13 2005; p 115.

45 – Girard OM, , Du J, Agemy L, Sugahara KN, Kotamraju VR, Ruoslahti E, Bydder GM, Mattrey RF. Optimization of iron oxide nanoparticle detection using ultrashort echo time pulse sequences: Comparison of T1, T2*, and synergistic T1 2 T2* contrast mechanisms. Magn Reson in Medicine. Accepted on November 18, 2010.

46 – Koch KM, Lorbiecki JE, Hinks RS, King KF. A multispectral three-dimensional acquisition technique for imaging near metal implants. Magn Reson Med 2009; 61:381-390.

47 – Lu W, Pauly KB, Gold GE, Pauly JM, Hargreaves BA. SEMAC: Slice encoding for metal artifact correction in MRI. Magn Reson Med 2009; 62:66-76.

48 – Cho ZH, Kim DJ, Kim YK. Total inhomogenity correction including chemical shifts and susceptibility by view angle tilting. Med Phys 1988; 15:7-11.

49 – Hargreaves BA, Chen W, Lu W, Alley MT, Gold GE, Brau AC, Pauly JM, Pauly KB. Accelerated slice encoding for metal artifact correction. J Magn Reson Imaging 2010; 31:987-96.

50 – Koch KM, Brau AC, Chen W et al. Imaging near metal with a MAVRIC-SEMAC hybrid. Magn Reson Med 2010 Oct 27 [Epub ahead of print].

51 – Rahmer J, Börnert P, Dries SP. Assessment of anterior cruciate ligament reconstruction using 3D ultrashort echo-time MR imaging. J Magn Reson Imaging 2009; 29:443-8.

52 – Wang K, Yu H, Brittain JH, Reeder SB, Du J. k-space water-fat decomposition with T2* estimation and multifrequency fat spectrum modeling for ultrashort echo time imaging. J Magn Reson Imaging 2010; 31:1027-34.

53 – Techawiboonwong A, Song HK, Leonard MB, Wehrli FW. Cortical bone water: in vivo quantification with ultrashort echo-time MR imaging. Radiology 2008; 248:824-833.

54 – Anumula S, Wehrli SL, Magland J, Wright AC, Wehrli FW. Ultra-short echo-time MRI detects changes in bone mineralization and water content in OVX rat bone in response to alendronate treatment. Bone 2010; 46:1391-9.

55 – Du J, Carl M, Bydder M, Takahashi A, Chung CB, Bydder GM. Qualitative and quantitative ultrashort echo time (UTE) imaging of cortical bone. J Magn Reson 2010; 207(2):304-11.

56 – Horch RA, Nyman JS, Gochberg DF, Dortch RD, Does MD. Characterization of ^{1}H NMR signal in human cortical bone for magnetic resonance imaging. Magn Reson Med 2010; 64:680-687.

57 – Keereman V, Fierens Y, Broux T et al. MRI-based attenuation correction for PET/MRI using ultrashort echo time sequences. J Nucl Med 2010; 51:812-8.

58 – Catana C, van der Kouwe A, Benner T et al. Toward implementing an MRI-based PET attenuation-correction method for neurologic studies on the MR-PET brain prototype. J Nucl Med 2010; 51:1431-8.

59 – Benjamin M, Milz S, Bydder GM. Magnetic resonance imaging of entheses. Part 1. Clin Radiol 2008; 63:691-703.

60 – Benjamin M, Milz S, Bydder GM. Magnetic resonance imaging of entheses. Part 2. Clin Radiol 2008; 63:704-711.

61 – Hauger O, Frank LR, Boutin RD *et al.* Characterization of the "red zone" of knee meniscus: MR imaging and histologic correlation. Radiology 2000; 217:193-200.

62 – Gatehouse PD, He T, Puri BK, Thomas RD, Resnick D, Bydder GM. Contrast-enhanced MRI of the menisci of the knee using ultrashort echo time (UTE) pulse sequences: imaging of the red and white zones. Br J Radiol 2004; 77:641-647.

63 – Bydder M, Rahal A, Fullerton GD, Bydder GM. The magic angle effect: a source of artifact, determinant of image contrast, and technique for imaging. J Magn Reson Imaging 2007; 25:290-300.

64 – Bydder GM, Chung CB. Magnetic resonance imaging of short T2 relaxation components in the musculoskeletal system. Skeletal Radiol 2009; 38:201-5.

65 – Bydder GM. Imaging of short and ultrashort T2 and T2 tissues using clinical MR systems. Imaging Med 2010; 2:225-233.

66 – Wang M, Radjenovic A, Stapleton TW et al. A novel and non-destructive method to examine meniscus architecture using 9.4 Tesla MRI. Osteoarthritis Cartilage 2010; 18:1417-20.

67 – Du J, Carl M, Diaz E, Takahashi A, Han E, Szeverenyi NM, Chung CB, Bydder GM. Ultrashort TE T1rho (UTE T1rho) imaging of the Achilles tendon and meniscus. Magn Reson Med 2010 64:834-42.

68 – Stehling C, Luke A, Stahl R et al. Meniscal T1rho and T2 measured with 3.0T MRI increases directly after running a marathon. Skeletal Radiol 2010 Oct 30. [Epub ahead of print].

69 – Gold GE, Thedens DR, Pauly JM *et al*. MR imaging of articular cartilage of the knee: new methods using ultrashort TEs. AJR Am J Roentgenol 1998; 170:1223-1226.

70 – Omoumi P, Teixeira P, Delgado G, Chung CB. Imaging of lower limb cartilage. Top Magn Reson Imaging 2009; 20:189-201.

71 – Koff MF, Potter HG. Noncontrast MR techniques and imaging of cartilage. Radiol Clin North Am. 2009; 47:495-504.

72 – Hall-Craggs MA, Porter J, Gatehouse PD, Bydder GM. Ultrashort echo time (UTE) MRI of the spine in thalassaemia. Br J Radiol 2004; 77:104-110.

73 – Messiou C, Collins DJ, Robson MD, Bydder GM, Morgan VA, deSouza NM. Quantifying sclerotic bone metastases with 2D ultra short TE MRI: a feasibility study. Cancer Biomarkers [in press].

74 – Hiwatashi A, Yoshiura T, Yamashita K, Kamano H, Honda H. Ultrashort TE MRI: Usefulness after percutaneous vertebroplasty. AJR Am J Roentgenol 2010; 195:W365-W368.

75 – Waldman A, Rees JH, Brock CS, Robson MD, Gatehouse PD, Bydder GM. MRI of the brain with ultra-short echo-time pulse sequences. Neuroradiology 2003; 45:887-92.

76 – Portman O, Flemming S, Cox JP, Johnston DG, Bydder GM. Magnetic resonance imaging of the normal pituitary gland using ultrashort TE (UTE) pulse sequences. Neuroradiology 2008; 50:213-20.

77 – Lehto LJ, Djaudat I, Corum CA, Garwood M, Gröhn OH. MRI detection of short T2 component in brain by SWIFT. Proc Int Soc Mag Reson Med 2010; 17:3326.

78 – Minty EP, Bjarnason TA, Laule C, MacKay AL. Myelin water measurement in the spinal cord. Magn Reson Med 2009; 61:883-92.

79 – Kolind SH, Mädler B, Fischer S, Li DK, MacKay AL. Myelin water imaging: Implementation and development at 3.0T and comparison to 1.5T measurements. Magn Reson Med 2009; 62:106-15.

80 – Macmillan EL, Mädler B, Fichtner N et al. Myelin water and T(2) relaxation measurements in the healthy cervical spinal cord at 3.0T: Repeatability and changes with age. Neuroimage 2011 Jan 15;54(2):1083-90. Epub 2010 Sep 9.

81 – Laule C, Vavasour IM, Leung E et al. Pathological basis of diffusely abnormal white matter: insights from magnetic resonance imaging and histology. Mult Scler 2010 Oct 21 [Epub ahead of print].

82 – Takahashi M, Togao O, Obara M et al. Ultra-short echo time (UTE) MR imaging of the lung: comparison between normal and emphysematous lungs in mutant mice. J Magn Reson Imaging 2010; 32:326-33.

83 – Togao O, Tsuji R, Ohno Y, Dimitrov I, Takahashi M. Ultrashort echo time (UTE) MRI of the lung: assessment of tissue density in the lung parenchyma. Magn Reson Med 2010 64:1491-8.

84 – Failo R, Wielopolski PA, Tiddens HA, Hop WC, Mucelli RP, Lequin MH. Lung morphology assessment using MRI: a robust ultra-short TR/TE 2D steady state free precession sequence used in cystic fibrosis patients. Magn Reson Med 2009; 61:299-306.

85 – Corum CA, Idiyatullin D, Moeller S, Chamberlain R, Sachdev D, Garwood M. Lung Imaging in the Mouse with SWIFT. Proc Int Soc Mag Res Med 2010; 17:204.

86 – Chappell KE, Patel N, Gatehouse PD et al. Magnetic resonance imaging of the liver with ultrashort TE (UTE) pulse sequences. J Magn Reson Imaging 2003; 18:709-13.

87 – Wansapura JP, Daniel BL, Vigen KK, Butts K. In vivo MR thermometry of frozen tissue using R2* and signal intensity. Acad Radiol 2005; 12:1080-1084.

88 – Kaye EA, Josan S, Lu A, Rosenberg J, Daniel BL, Pauly KB. Consistency of signal intensity and T2* in frozen ex vivo heart muscle, kidney, and liver tissue. J Magn Reson Imaging 2010; 31:719-24.

89 – Chan CF, Keenan NG, Nielles-Vallespin S et al. Ultra-short echo time cardiovascular magnetic resonance of atherosclerotic carotid plaque. J Cardiovasc Magn Reson 2010;12:17.

90 – Sharma S, Boujraf S, Bornstedt A et al. Quantification of calcification in endarterectomy samples by means of high-resolution ultra-short echo time imaging. Invest Radiol 2010; 45:109-13.

91 – Du J, Corbeil J, Znamirowski R et al. Direct imaging and quantification of carotid plaque calcification. Magn Reson Med 2010 Nov 30 [Epub ahead of print].

92 – Robson MD, Gatehouse PD, So PW, Bell JD, Bydder GM. Contrast enhancement of short T2 tissues using ultrashort TE (UTE) pulse sequences. Clin Radiol 2004; 59:720-6.

93 – Tymofiyeva O, Boldt J, Rottner K, Schmid F, Richter EJ, Jakob PM. High-resolution 3D magnetic resonance imaging and quantification of carious lesions and dental pulp in vivo. MAGMA 2009; 22:365-374.

94 – Djaudat I, Corum CA, Moeller S, Prasad HS, Garwood M, Nixdorf DR. SWIFT versus X-ray in dental imaging. Proc Int Soc Mag Reson Med 2010; 17:543.

95 – Rühli FJ, von Waldburg H, Nielles-Vallespin S, Böni T, Speier P. Clinical magnetic resonance imaging of ancient dry human mummies without rehydration. JAMA 2007; 298:2618-20.

96 – Ra, JB, Hilal SK, Cho ZH. A method for in vivo MR imaging of the short T2 component of sodium-23. Magn Reson Med 1986; 3:296-302.

97 – Nielles-Vallespin S, Weber MA, Bock M et al. 3D radial projection technique with ultrashort echo times sodium MRI: clinical applications in human brain and skeletal muscle. Magn Reson Med 2007; 57:74-81.

98 – Atkinson IC, Sonstegaard R, Pliskin NH, Thulborn KR. Vital signs and cognitive function are not affected by 23-sodium and 17-oxygen magnetic resonance imaging of the human brain at 9.4T. J Magn Reson Imaging 2010; 32:82-7.

99 – Lu A, Atkinson IC, Claiborne TC, Damen FC, Thulborn KR. Quantitative sodium imaging with a flexible twisted projection pulse sequence. Magn Reson Med 2010; 63:1583-93.

100 – Atkinson IC, Thornton KR. Feasibility of mapping the tissue mass corrected bioscale of cerebral metabolic rate of oxygen consumption using 17-oxygen and 23-sodium MR imaging in a human brain at 9.4 T. Neuroimage 2010; 51:723-33.

101 – Ouwerkerk R, Bottomley PA, Solaiyappan M, Spooner AE, Tomaselli GF, Wu KC, Weiss RG. Tissue sodium concentration in myocardial infarction in humans: a quantitative 23Na MR imaging study. Radiology 2008; 248:88-96.

102 – Madelin G, Lee JS, Inati S, Jerschow A, Regatte RR. Sodium inversion recovery MRI of the knee joint in vivo at 7T. J Magn Reson 2010; 207:42-52.

103 – Wang L, Wu Y, Chang G et al. Rapid isotropic 3D-sodium MRI of the knee joint in vivo at 7T. J Magn Reson Imaging 2009; 30:606-14.

104 – Chang G, Wang L, Schweitzer ME, Regatte RR. 3D 23Na MRI of human skeletal muscle at 7 Tesla: initial experience. Eur Radiol 2010; 20:2039-46.

105 – Robson MD, Tyler DJ, Neubauer S. Ultrashort TE chemical shift imaging (UTE-CSI). Magn Reson Med 2005; 53:267-274.

106 – Qian Y, Williams AA, Chu CR, Boada FE. Multicomponent T2* mapping of knee cartilage: technical feasibility ex vivo. Magn Reson Med 2010; 64:1426-31.

107 – Williams A, Qian Y, Bear D, Chu CR. Assessing degeneration of human articular cartilage with ultra-short echo time (UTE) T2* mapping. Osteoarthritis Cartilage 2010; 18:539-46.

108 – Filho GH, Du J, Pak BC et al. Quantitative characterization of the Achilles tendon in cadaveric specimens: T1 and T2* measurements using ultrashort-TE MRI at 3 T. AJR Am J Roentgenol 2009; 192:W117-24.

109 – Du J, Pak BC, Znamirowski R et al. Magic angle effect in magnetic resonance imaging of the Achilles tendon and enthesis. Magn Reson Imaging 2009; 27:557-64.

110 – Szeverenyi NM, Bydder GM. Dipolar anisotropy fiber imaging in a goat knee meniscus. Magn Reson Med 2010 Oct 11. [Epub ahead of print].

111 – Atkinson IC, Lu A, Thulborn KR. Characterization and correction of system delays and eddy currents for MR imaging with ultrashort echo-time and time-varying gradients. Magn Reson Med 2009; 62:532-7.

112 – Josan S, Pauly JM, Daniel BL, Pauly KB. Double half RF pulses for reduced sensitivity to eddy currents in UTE imaging. Magn Reson Med 2009; 61:1083-9.

113 – Josan S, Kaye E, Pauly JM, Daniel BL, Pauly KB. Improved half RF slice selectivity in the presence of eddy currents with out-of-slice saturation. Magn Reson Med. 2009; 61:1090-5.

114 – Paley MNJ, Kruykov E, Lamperth M et al. An independent multichannel imaging research system for ultrashort echo time imaging on clinical MR systems. Concepts Mag Reson Part B: Mag Reson Eng 2009; 35B:80-88.

115 – Gurney PT, Hargreaves BA, Nishimura DG. Design and analysis of a practical 3D cones trajectory. Magn Reson Med 2006; 55:575-82.

116 – Du J, Bydder M, Takahashi AM, Chung CB. Two-dimensional ultrashort echo time imaging using a spiral trajectory. Magn Reson Imaging 2008; 26:304-12.

117 – Hetzer S, Mildner T, Möller HE. A Modified EPI sequence for high-resolution imaging at ultra-short echo time. Magn Reson Med 2010 Sep 27. [Epub ahead of print].

118 – Larson PE, Conolly SM, Pauly JM, Nishimura DG. Using adiabatic inversion pulses for long-T2 suppression in ultrashort echo time (UTE) imaging. Magn Reson Med 2007; 58:952-61.

119 – Larson PE, Gurney PT, Nayak K, Gold GE, Pauly JM, Nishimura DG. Designing long-T2 suppression pulses for ultrashort echo time imaging. Magn Reson Med 2006; 56:94-103.

120 – Carl M, Bydder M, Du J, Han E. Radiofrequency pulses for simultaneous short T(2) excitation and long T(2) suppression. Magn Reson Med 2010 Sep 24. [Epub ahead of print].

121 – Carl M, Bydder M, Du J, Takahashi A, Han E. Optimization of RF excitation to maximize signal and T2 contrast of tissues with rapid transverse relaxation. Magn Reson Med 2010; 64(2):481-90.

122 – Du J, Takahashi AM, Bea WC, Chung CB, Bydder GM. Dual inversion recovery, ultrashort echo time (DIR UTE) imaging: creating high contrast for short-T(2) species. Magn Reson Med 2010; 63:447-55.

123 – Du J, Takahashi AM, Bydder M, Chung CB, Bydder GM. Ultrashort TE imaging with off-resonance saturation contrast (UTE-OSC). Magn Reson Med 2009; 62:527-31.

124 – Rahmer J, Blume U, Börnert P. Selective 3D ultrashort TE imaging: comparison of "dual-echo" acquisition and magnetization preparation for improving short-T2 contrast. MAGMA 2007; 20:83-92.

125 – Nestrasil I, Michaeli S, Liimatainen T, Rydeen CE, Kotz CM, Nixon JP, Hanson T, Tuite PJ. T1rho and T2rho MRI in the evaluation of Parkinson's disease. J Neurol 2010; 257:964-8. Epub 2010 Jan 8.

126 – O'Brien KR, Myerson SG, Cowan BR, Young AA, Robson MD. Phase contrast ultrashort TE: A more reliable technique for measurement of high-velocity turbulent stenotic jets. Magn Reson Med 2009; 62:626-36.

LEGENDS TO FIGURES

Fig 1 UTE MR Image of the Skull. The inner and outer tables of the skull are seen in a manner similar to x-ray computed tomography with bone windows.

Fig 2 UTE image of the Achilles tendon. Oblique fibers are seen within the tendon (arrows).

Fig 3 Short TE Image of the Meniscus. The lamellar layer, radial and vertical fibers are seen. Circumferential fibers are of low intensity.

Fig 1 - Skull

UTE Subtraction

UTE Subtraction

Fig 2
Achilles Tendon Oblique, Spiral Fibers

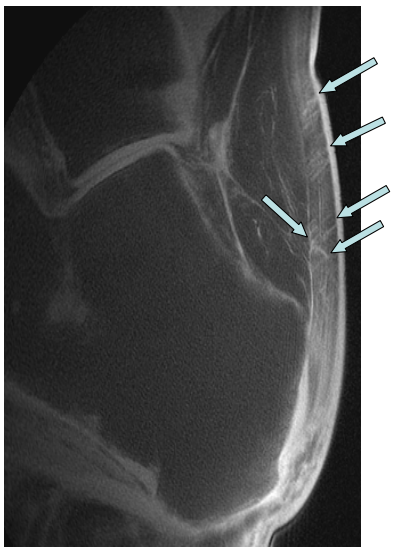

Fig 3 - Meniscus